



Copper Catalysts Supported on Barium Deficient Perovskites for CO Oxidation Reaction

A. Díaz-Verde¹ · V. Torregrosa-Rivero¹ · M. J. Illán-Gómez¹

Accepted: 10 October 2022
© The Author(s) 2022

Abstract

Mixed oxides with perovskite-type structure (ABO_3) present interesting physico-chemical properties to be used as catalyst for atmospheric pollution control. In this work, a series of $CuX/Ba_{0.7}MnO_3$ catalysts (being x : 0, 4, 8 and 12 wt%) has been synthesized, characterized and tested for CO oxidation reaction. All the catalysts were active for CO oxidation in the two reactant mixtures tested: low CO mixture (0.1% CO and 1% O_2 in He) and near stoichiometric mixture (1% CO and 1% O_2 in He). Copper-free perovskite is the most active catalyst in the less demanding conditions (0.1% CO and 1% O_2), as it presents the highest amount of oxygen vacancies working as active sites. However, at higher CO concentrations (1% CO in near stoichiometric mixture), copper-containing catalysts were more active than the perovskite support because, due to the saturation of the oxygen vacancies of perovskites, CuO seems to participate as active site for CO and O_2 activation. $Cu4/Ba_{0.7}MnO_3$ and $Cu12/Ba_{0.7}MnO_3$ are more active than $Cu8/Ba_{0.7}MnO_3$ catalyst, since they present a larger amount of active sites on surface. These two copper-containing catalysts present a high stability and recyclability during the reaction at 300 °C in an ideal near stoichiometric mixture (1% CO and 1% O_2).

Keywords Perovskite · Copper · Manganese · CO oxidation

1 Introduction

Nowadays, global greenhouse gas emissions still presenting very high levels that seem not to have reached their maximum. As a consequence, the average temperature on Earth is 1.1 °C higher than the recorded at the end of the nineteenth century [1]. In fact, one of the most significant conclusions achieved by the Paris Agreement was to limit the increase in the average temperature on Earth (respect to pre-industrial levels) to a maximum of 1.5 °C. To reach this purpose, quite ambitious measures have to be turned out [2], being some of them currently applied, such as, among others, the limitation of the use of diesel vehicles as well as the transition towards electric vehicles and those based on fuel cells. However, it is foreseeable that gasoline vehicles will not be completely replaced in 2040 [3]. As some of the pollutants generated by gasoline vehicles cause several environmental and health

problems, the design of effective catalysts to control the composition of exhaust gases generated by these engines will continue being a challenging issue [4].

To accomplish the current and future legislation, it is required the development of a new generation of three-way catalysts (TWCs) presenting, among other characteristics, higher activities at lower temperatures than current TWCs [5]. An example is the challenging objective called “Target 150”, which implies achieving a 90% reduction in HC, CO and NO_x emissions at 150 °C. The new catalytic systems to be developed must present high Oxygen Storage Capacities (OSC), to avoid unwanted NO_x and CO emissions, and a very high stability which assures the minimal deactivation during the useful life. Additionally, in the formulation of these new TWCs, the use of noble metals (mainly Pt, Pd and Rh) has to be minimized as much as possible. In this sense, mixed oxides with perovskite-type structure (ABO_3) [6–9] are considered as an interesting family of catalysts for the fulfillment of the above mentioned objectives.

Recently, the authors analyzed the activity for CO oxidation of a series of under-stoichiometric Ba_xMnO_3 perovskites, concluding that $Ba_{0.7}MnO_3$ is the best catalyst due to the presence of a high amount of oxygen vacancies working

✉ M. J. Illán-Gómez
illan@ua.es

¹ Carbon Materials and Environment Research Group, Inorganic Chemistry Department, University of Alicante, Alicante, Spain

as active sites [10]. Additionally, the high selectivity to CO₂ found for a series of BaMn_{1-x}Cu_xO₃ perovskites used for diesel-soot oxidation revealed a high capacity to oxidize CO to CO₂ [11]. Based on these statements, in this paper, a series of copper-containing catalysts supported on Ba_{0.7}MnO₃ have been synthesized, characterized and tested for CO oxidation reaction in ideal conditions that simulate the required for the new TWCs. The samples have been referred as B0.7M for the raw perovskite used as support (Ba_{0.7}MnO₃), and as CuX/B0.7M for the impregnated perovskites, where X indicates the nominal weight percentage of Cu in the catalysts (4, 8 and 12 wt%).

2 Experimental

2.1 Synthesis and Characterization of Catalysts

The Ba_{0.7}MnO₃ perovskite used as support (B0.7M) was synthesized using the sol–gel method adapted to aqueous medium [12, 13]. Briefly, a 40 mL solution (containing EDTA as chelating agent in a 1:2 molar Mn:EDTA ratio) at 60 °C was prepared. Ba(NO₃)₂ and Mn(NO₃)₂*4 H₂O were added as metal precursors and, after, citric acid was incorporated using the same molar ratio (1:2, Mn: citric acid). Subsequently, the temperature was increased to 80 °C for assuring the gel formation. The described procedure was carried out keeping the pH in 9 by employing an ammonia solution (30% wt). Finally, the obtained gel was dried at 150 °C during 12 h and, as the last step, the solid was calcined at 850 °C for 6 h.

For copper addition to perovskite support, the incipient wetness impregnation method was used. For that, the support was kept in contact with the volume of a Cu(NO₃)₂*3 H₂O solution (with a concentration depending on the Cu amount) needed to wet the solid. The wet catalyst is stirred at room temperature during 24 h, dried at 90 °C during 24 h and, finally, calcined at 600 °C during 3 h.

For sample characterization, the following techniques have been employed.

The copper content was measured by ICP-OES on a Perkin-Elmer device model Optimal 4300 DV. For this analysis, the elements were extracted by the mineralization of the samples using a diluted aqua regia solution (HNO₃:HCl, 1:3) and stirring at 60 °C for 1 h.

The textural properties were determined by N₂ adsorption at – 196 °C using an Autosorb-6B instrument from Quantachrome (Anton Paar Austria GmbH). The samples were degassed at 250 °C for 4 h before the N₂ adsorption experiments.

The crystalline structure was obtained using X-ray Diffraction (XRD). The X-ray patterns were recorded between 20 and 80° 2θ angles with a step rate of 0.4°/min and using

Cu K_α (0.15418 nm) radiation in a Bruker D8-Advance device. FT-IR spectra from 4000 to 500 cm⁻¹ were also obtained using a BRUKER IFS 66/S apparatus and with a spectral resolution of 4 cm⁻¹.

The morphology of catalysts was analyzed by electronic microscopy, using a ZEISS Merlin VP Compact for Field Emission Scanning Electronic Microscopy (FE-SEM).

The surface chemistry was assessed by X-ray Photoelectron Spectroscopy (XPS) using a K-Alpha Photoelectron Spectrometer by Thermo-Scientific with an Al K_α (1486.7 eV) radiation source. To obtain XPS spectra, the pressure of the analysis chamber was maintained at 5 × 10⁻¹⁰ mbar. The binding energy (BE) and kinetic energy (KE) scales were adjusted by setting the C 1 s transition at 284.6 eV, and the BE and KE values were then determined with the peak-fit software of the spectrometer. The O_L/(Ba + Mn), O_{def}/(Ba + Mn), Cu/(Ba + Mn + Cu), and Mn(IV)/Mn(III) XPS ratios were calculated using the area under the suggested deconvoluted bands of O 1 s, Mn 2p^{3/2}, Cu 2p^{3/2} and Ba 3d^{5/2}.

Reducibility of catalysts was determined by Temperature Programmed Reduction with H₂ (H₂-TPR) in a Pulse Chemisorb 2705 (from Micromeritics) provided by a Thermal Conductivity Detector (TCD) and using 30 mg of sample which was heated at 10 °C/min from 25 to 1000 °C in 5% H₂/Ar atmosphere (40 mL/min). The quantification of the H₂ consumption was carried out using a CuO reference sample.

O₂-TPD experiments were performed in a TG-MS (Q-600-TA and Thermostar from Balzers Instruments (Pfeiffer Vacuum GmbH, Germany) respectively), with 16 mg of sample heated at 10 °C/min from room temperature to 950 °C under a 100 mL/min of helium atmosphere. 18, 28, 32 and 44 m/z signals were followed for H₂O, CO, O₂ and CO₂ (respectively) evolved during the experiments. The amount of evolved oxygen was estimated using a CuO reference sample and the weight data recorded by the TG system was used to obtain the mass loss profiles.

2.2 Activity Tests

To determine the catalytic activity for CO oxidation, Temperature-Programmed Reaction experiments (CO-TPR) have been developed using two ideal reactant mixtures composed by: (i) 0.1% CO and 1% O₂ in He (low CO reactant mixture) and (ii) 1% CO and 1% O₂ in He (near stoichiometric reactant mixture, which simulates the CO concentration in the actual TWC working conditions). For the experiments, 50 mg of catalysts and 100 mg of SiC were loaded into a U-shape quartz reactor, and a 10 °C/min heating rate from room temperature to 500 °C has been applied. The mixture catalyst-SiC is pre-heated for 1 h at 600 °C in a 5% O₂/He gas mixture to clean the surface of the catalysts. The most active catalysts were also tested at 300 °C during 5 h, using the near stoichiometric reactant

mixture. In order to determine the recyclability of catalysts, two reaction cycles were developed. For reaction products quantification, a HP6890 gas chromatograph, provided with a Thermal Conductivity Detector and two packed columns (Porapak-Q and MolSieve-13X), was used.

The CO conversion was determined using the following equation.

$$\text{CO conversion (\%)} = \frac{(\text{CO}_{\text{in}} - \text{CO}_{\text{out}})}{\text{CO}_{\text{in}}} \cdot 100$$

3 Results and Discussion

3.1 Chemical, Morphological and Structural Characterization

Table 1 features the BET surface area, determined by N₂ adsorption, and the copper content (nominal and actual

obtained using ICP-OES) of the B0.7M and CuX/B0.7M catalysts. All samples present very low surface areas, as expected for solids with an almost negligible porosity as perovskite mixed oxides are [14, 15]. As expected for impregnated samples, actual and nominal copper content are closer at low metal loadings than at high copper loadings.

Figure 1a shows the X-ray patterns of the B0.7M and CuX/B0.7M catalysts. The bare support exhibits a hexagonal BaMnO₃ perovskite structure, which is also identified after copper loading. In a previous study, it has been concluded that due to copper insertion into the perovskite lattice, the hexagonal perovskite structure is modified to a BaMnO₃ polytype structure [11], as the difference between manganese and copper ratios modifies the chemical bond lengths [16]. Thus, as polytype structure is not identified for CuX/B0.7M catalysts series, it seems that copper has not been inserted into the perovskite lattice. Figure 1b shows the FT-IR spectra for CuX/B0.7M catalysts and for the B0.7M perovskite used as support, where the following peaks are identified: (i) from 500 to 786 cm⁻¹, associated to the stretching vibration of

Table 1 Specific surface area, copper content and XRD data values for B0.7M and CuX/B0.7M catalysts

| Catalyst | BET surface area (m ² /g) | Nominal Cu (wt%) | Actual Cu (wt%) | Cell parameters (Å) ^a | | Average crystal size (nm) |
|------------|--------------------------------------|------------------|-----------------|----------------------------------|------|---------------------------|
| | | | | a | c | |
| B0.7M | 5 | – | – | 5.68 | 4.82 | 18.24 |
| Cu4/B0.7M | 12 | 4 | 4 | 5.69 | 4.80 | 15.24 |
| Cu8/B0.7M | 5 | 8 | 7 | 5.69 | 4.81 | 12.60 |
| Cu12/B0.7M | 6 | 12 | 9 | 5.69 | 4.79 | 12.72 |

^aCalculated using the main XRD hexagonal perovskite peak

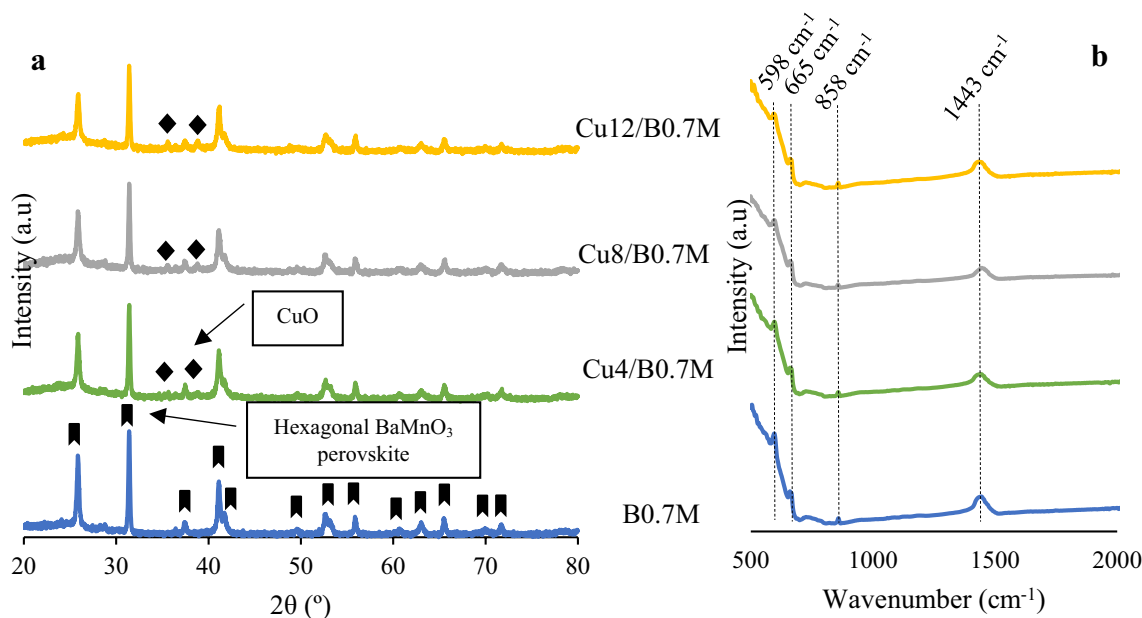


Fig. 1 XRD patterns (a) and FT-IR spectra (b) of B0.7M and CuX/B0.7M catalysts

Mn–O bonds in the MnO_6 octahedra of perovskite structure, and (ii) at 858 and 1443 cm^{-1} , corresponding to the asymmetric stretching of the carbonate ion, which confirms the presence of BaCO_3 [36–38].

The average crystallite size and the cell parameters of the hexagonal perovskite phase ($a = b \neq c$) have been calculated using the Williamson-Hall method [17], being the values included in Table 1. The data reveal that the average crystallite size of perovskite decreases as copper content increases, achieved a minimum value for Cu8/B0.7M and Cu12/B0.7M . So, as observed for other copper-containing perovskites [11], the presence of copper seems to hinder the crystal growth. For CuX/B0.7M catalysts, a slight distortion of the hexagonal structure is featured because c parameter decreases respect to bare perovskite (B0.7M). However, this distortion seems not to directly depend on the copper content as it is similar for the two copper containing catalysts with higher copper content (Cu8/B0.7M and Cu12/B0.7M).

Note that in CuX/B0.7M catalysts, the very low intensity of tenorite peaks for CuO species (observed at 35.6° and

$38.8^\circ 2\theta$ values in Fig. 1a) seem to reveal that copper is so well dispersed on the perovskite surface that the average crystal size is close to the detection limit of the XRD technique [18]. Otherwise, it also could indicate that the CuO phase is not crystalline. In Fig. 1b, the CuO phase existing in the catalysts should feature the stretching vibration peaks of the Cu–O bond at 433 , 508 and 606 cm^{-1} [39], however, these active modes are not detected as they are located in the same wavenumber range than perovskite modes.

Finally, the FE-SEM images of catalysts shown in Fig. 2 reveal the presence of amorphous particles with different sizes that hinders the measure of the average particle size and, consequently, the particle size distribution cannot be obtained. Note that a significant effect of copper on the morphology of catalysts is not detected.

3.2 Surface Properties

XPS analysis provides information about the surface composition of catalysts. The experimental profiles (colored line)

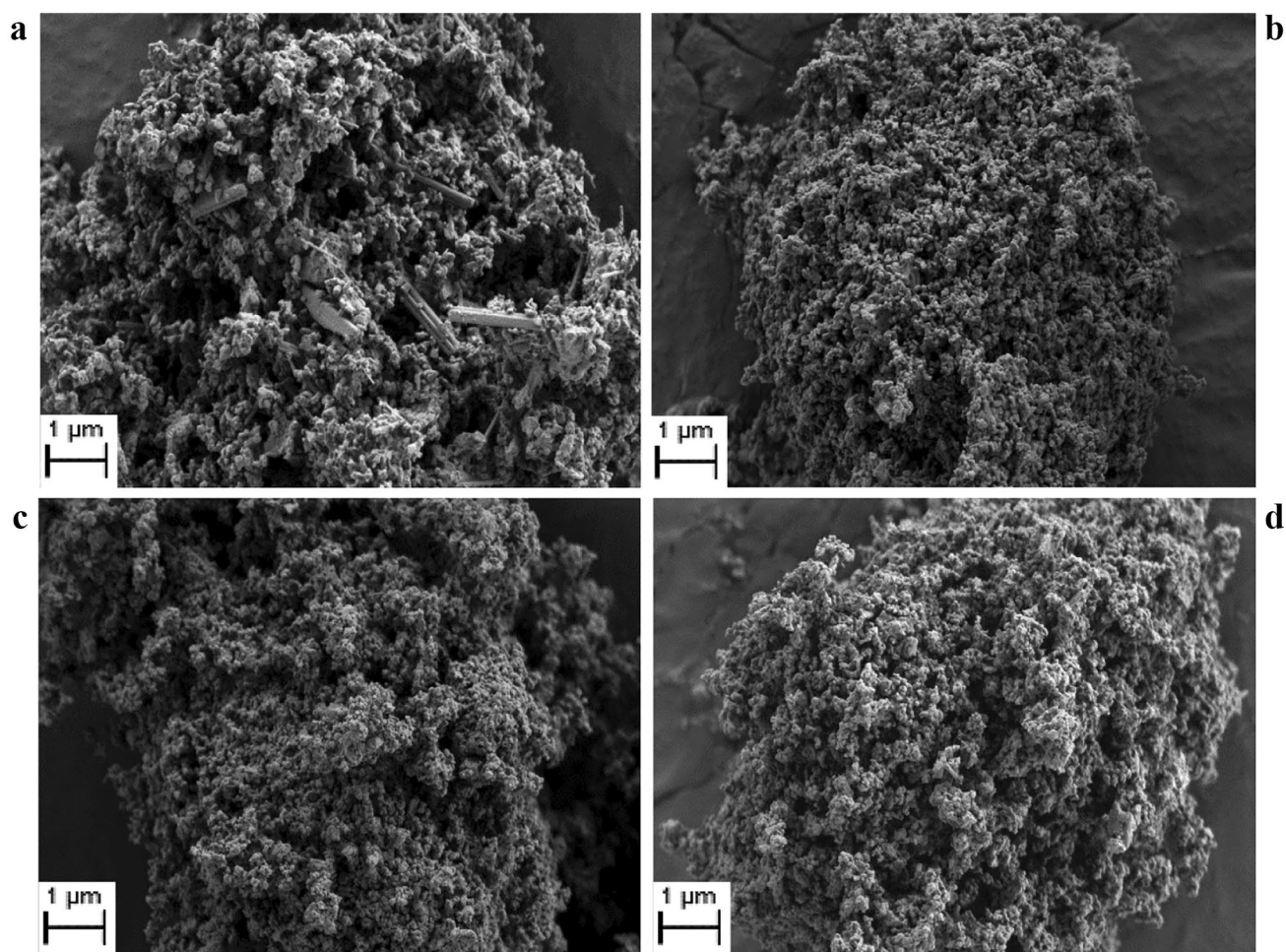


Fig. 2 FE-SEM images of B0.7M **a** Cu4/B0.7M **b**, Cu8/B0.7M **c** and Cu12/B0.7M **d** catalysts

have been included to show the accuracy of the deconvolutions (black lines). Figure 3a displays the Mn $2p_{3/2}$ XPS spectra, where the following contributions can be found: (i) Mn(III) at lower binding energies with maximum at around 640 eV (ranging from 639.70 eV for Cu4/B0.7M to 641.60 eV for B0.7M), and (ii) Mn(IV) at higher binding energies with a maximum at ca. 642 eV (from 642 eV for Cu4/B0.7M to 642.70 eV for B0.7M). The presence of the satellite peak at 644 eV confirms that Mn(III) exists on the perovskite surface [19–21]. The Mn(IV)/Mn(III) ratios, calculated using the corresponding area under the deconvoluted peaks and shown in Table 2, reveal that the support presents a higher amount of Mn(III) than of Mn(IV) on surface and that, after the addition of copper, the amount of Mn(IV) notably increases as the Mn(IV)/Mn(III) ratio is higher than 1. This trend, which is also observed when cation defects exist on the perovskite surface [10], is the result of the oxidation mechanism [a fraction of Mn(III) is oxidized to Mn(IV)] taking place to achieve the electroneutrality due to the presence of Cu(II) on surface [22]. A shift in the position of the maximum of Mn(IV) and Mn(III) peaks is detected for the CuX/B0.7M catalysts respect to the B0.7M support, as consequence of the higher electronic density in the Mn environment due to its contact with Cu. In fact, for copper-impregnated samples, the Mn(III) deconvoluted peak (continuous black line) is divided into two contributions that could correspond with Mn(III) species close to Cu (named as Mn(III)_c in Fig. 3a) and those far from Cu (named as Mn(III)_f) in Fig. 3a) and those far from Cu (named as Mn(III)_f). Note

Table 2 Mn and Cu XPS characterization data in the fresh catalysts

| Catalyst | Mn(IV)/Mn(III) | Mn(III) _c /Mn(III) _f | XPS Cu/(Ba + Mn + Cu) (nominal) | Cu _{si} /Cu _{wi} |
|------------|----------------|--|---------------------------------|------------------------------------|
| B0.7M | 0.5 | – | – | – |
| Cu4/B0.7M | 1.3 | 0.2 | 0.10 (0.07) | 1.6 |
| Cu8/B0.7M | 1.3 | 0.3 | 0.12 (0.10) | 0.8 |
| Cu12/B0.7M | 1.4 | 0.2 | 0.18 (0.15) | 1.3 |

that the values of Mn(III)_c/Mn(III)_f ratio in Table 2 seem not to significantly depend of the copper content.

In the O 1s transition spectra recorded for all the catalysts shown in Fig. 3b, four different contributions can be identified: (i) the lattice oxygen (O_L), corresponding to the band located at binding energy values between 528 and 529 eV, (ii) oxygen vacancies (O_{def}), corresponding to defect sites with low oxygen coordination, associated to the band located at approximately 531 eV, (iii) adsorbed oxygen, hydroxyl and carbonate groups, that appear at 532 eV, and (iv) chemisorbed water at binding energies over 533 eV [19, 23–27]. This last band has been only detected for the bare perovskite (B0.7M), as during the thermal treatment used in the incipient wetness impregnation, the moist has been removed. Note that the lattice oxygen contribution of the impregnated catalysts is divided in two peaks that could correspond to the lattice oxygen of the perovskite and of the CuO phase. By

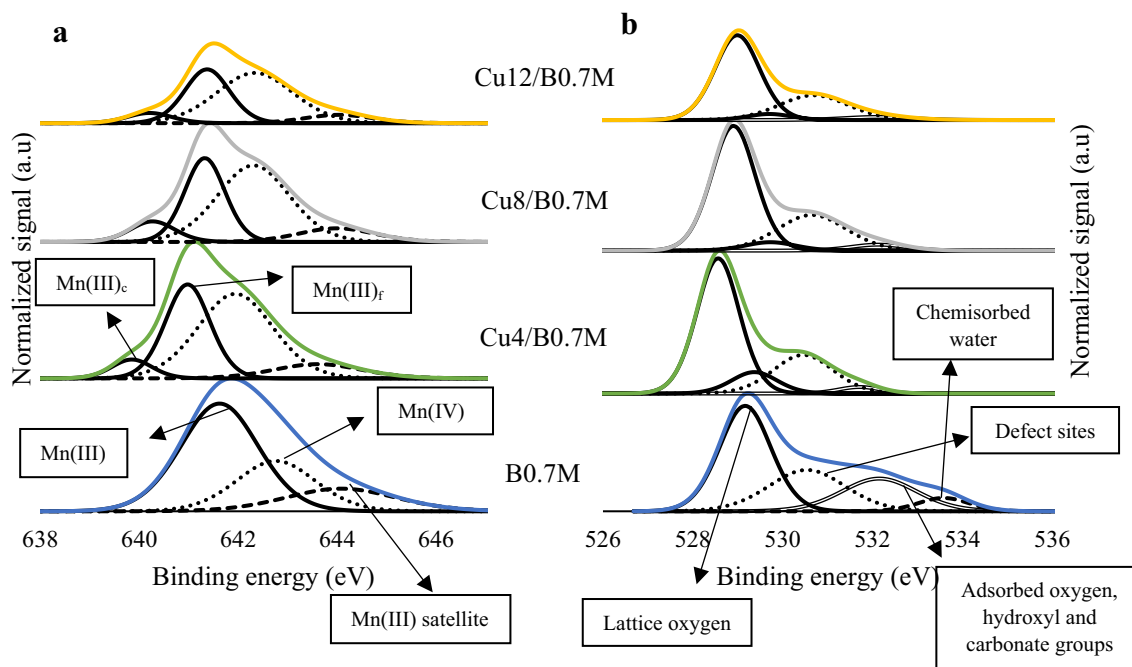


Fig. 3 XPS spectra of the Mn $2p_{3/2}$ **a** and O 1s **b** transitions

comparing the $O_L/(Ba + Mn)$ XPS ratios included in Table 3 with the nominal value (1.76 for $Ba_{0.7}MnO_3$ perovskite), information about the presence of oxygen vacancies on the catalysts surface can be obtained. Thus, oxygen defects are present in all catalysts, because the experimental ratios are lower than the nominal one, but a slight decrease is featured for CuX/B0.7M catalysts as the $O_L/(Ba + Mn)$ ratio is higher than in B0.7M. Note that the lower amount of oxygen vacancies in the copper catalysts is confirmed by the decrease in the $O_{def}/(Ba + Mn)$ ratio (see Table 3) which, however, seems not to be significantly affected by the Cu percentage.

Finally, the XPS profiles corresponding to the Cu $2p_{3/2}$ transition are presented in Fig. 4. For reduced copper species [such as Cu(I) and Cu(0)] a XPS signal at binding energy values below 933 eV is expected and, for Cu(II) species, the XPS signal appears at binding energies over 933 eV, which also has to present satellite peaks at 940 eV and 943 eV [19, 24]. As in Fig. 3, a signal around 933 eV is detected for all copper containing catalysts (as well as the satellite peak), Cu(II) seems to be present at the catalysts surface. The Cu4/B0.7M catalyst shows a XPS band at binding energies slightly below 933 eV, probably due to a rich electronic density around Cu due to the charge transfer from an electropositive atom as barium [19, 23, 24, 28] which affects more to this catalyst due its lowest Cu content. As found for other copper-containing perovskites [10–12, 26, 29], in the Cu(II) band for all CuX/B0.7M catalysts two different

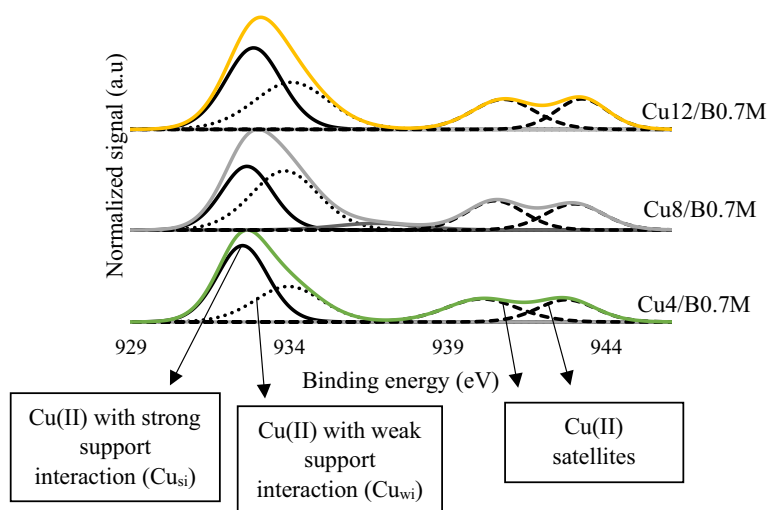
contributions are found: (i) the signal located at lower binding energies which corresponds with surface Cu(II) species with a stronger interaction with the perovskite support (Cu_{si}), thus, presenting a higher electronic density in their environment, and (ii) the signal placed at higher binding energies, which is associated with surface Cu(II) ions with a weaker interaction with the perovskite (Cu_{wi}) [10–12, 26, 29]. The proportion of these two contributions (showed in Table 2 as Cu_{si}/Cu_{wi} ratio) depends on the copper content, being Cu8/B0.7M the catalyst showing the lowest proportion of copper with a strong interaction with perovskite.

To obtain information about the distribution of copper in the catalyst, XPS value and nominal value of Cu/(Ba + Mn + Cu) ratio (calculated based on the areas of the XPS signals and on the nominal metal contents of the catalyst formula, respectively) are compared [10–12, 26, 29]. A Cu/(Ba + Mn + Cu) XPS ratio value higher than the nominal one is expected if CuO phase is being accumulated on the catalyst surface, and the opposite will indicate that copper is inserted into the lattice. Therefore, as Cu/(Ba + Mn + Cu) XPS ratio is higher than the nominal one for all the catalysts, it seems that the copper (as CuO) located on the surface is the main copper species. Note that the Cu4/B0.7M catalyst presents the highest CuO accumulation on the perovskite surface as the XPS ratio is 1.4 times higher than the nominal, meanwhile it is 1.2 times for Cu8/B0.7M and for Cu12/B0.7M. This is consistent with the more pronounced O_L band corresponding to CuO phase identified in the O 1s XPS spectrum (Fig. 3b) of Cu4/B0.7M.

Table 3 Oxygen XPS characterization data in the fresh catalysts

| Catalyst | $O_L/(Ba + Mn)$ | $O_{def}/(Ba + Mn)$ |
|------------|-----------------|---------------------|
| B0.7M | 1.2 | 0.7 |
| Cu4/B0.7M | 1.4 | 0.2 |
| Cu8/B0.7M | 1.2 | 0.1 |
| Cu12/B0.7M | 1.3 | 0.1 |

Fig. 4 XPS spectra of the Cu $2p_{3/2}$ transition



3.3 Redox Properties

Reducibility and redox properties of catalysts were analyzed by Temperature Programmed Reduction with H_2 (H_2 -TPR), being the H_2 consumption profiles shown in Fig. 5a, including the H_2 profile for CuO used as a reference. In the H_2 -TPR

profiles, several peaks are identified [10–12, 26, 29]. For the perovskite support (B0.7M), a peak between 420 °C and 480 °C corresponding to the Mn(IV) and Mn(III) reduction to Mn(II) is found. The intensity of this peak increases with the Cu amount, and its maximum is shifted to temperatures between 210 and 340 °C for copper-supported catalysts suggesting a Mn-Cu synergic effect. For the CuO reference, the peak at temperatures between 200 and 370 °C corresponds to Cu(II) reduction to Cu(0). Thus, the peak for Cu reduction in the CuX/B0.7M catalysts is overlapped with the corresponding to Mn(IV) and Mn(III) reduction [11]. A similar synergic effect between Cu and B metal in perovskite has been observed by Zhang et al. [31] for $\text{LaFe}_{1-x}\text{Cu}_x\text{O}_3$ perovskites and by Torregrosa-Rivero et al. for $\text{BaFe}_{1-x}\text{Cu}_x\text{O}_3$ perovskites [14]. Finally, the very small peak at around 730 °C corresponds to the reduction of oxygen species on the catalysts surface, meanwhile, at around 850 °C, it is detected a very small peak corresponding to the reduction of bulk Mn(III) to Mn(II).

In Fig. 5b, the nominal H_2 consumption calculated considering that manganese [as Mn(III) or Mn(IV)] is reduced to Mn(II) and that Cu(II) is reduced to Cu(0), is compared with the experimental H_2 consumption (determined from the area under the H_2 -TPR profiles). All the experimental values are closer to the nominal one corresponding to Mn(III) and Cu(II), even though the values are lower. Thus, it seems that Mn(III) is the main oxidation state in the bulk catalysts. However, according to XPS results, the Mn(IV) is the main oxidation state on the surface for CuX/B0.7M catalysts, and this is because the presence of the CuO phase on surface promotes the oxidation of Mn(III) to Mn(IV). A

similar conclusion has been published by Wang et al. [30] for $\text{La}_{0.8}\text{Sr}_{0.2}\text{MnO}_{3.15}$ perovskites.

3.4 O_2 Release During a Temperature Programmed Desorption in He (O_2 -TPD)

The profiles corresponding to the O_2 released by catalysts during a TPD in He are shown in Fig. 6a. Three peaks are usually observed for perovskites [31–33]: (i) a low temperature peak, between 150 and 350 °C, due to the desorption of oxygen adsorbed on surface vacancies (α - O_2); (ii) a medium temperature peak, from 350 to 700 °C, where the desorbed oxygen comes from the adsorbed on the lattice defects (α' - O_2); and (iii) at high temperature peak over 700 °C, which corresponds to the release of lattice oxygen (β - O_2), which is related with the Mn(IV) to Mn(III) reduction and with the presence of oxygen defects that facilitate the desorption. This high temperature peak informs about the lattice oxygen mobility though perovskite which is related with oxidation ability [10, 11].

For all perovskites, the O_2 desorbed corresponds mainly to lattice oxygen (β - O_2). B0.7M perovskite shows also a very small O_2 desorption at around 600 °C, corresponding to α' - O_2 , which is due to oxygen adsorbed on the lattice defects. For CuX/B0.7M catalysts the profile of β - O_2 shows also a peak at lower temperatures, whose intensity increases with the copper percentage. This suggests that it could be related with the presence of CuO phase, so it could correspond to lattice oxygen from tenorite phase. In fact, the Cu4/B0.7M catalyst, which evolves the lowest β - O_2 at lower temperatures, presents the highest CuO accumulation on the perovskite support [based on Cu/(Ba + Mn + Cu) XPS

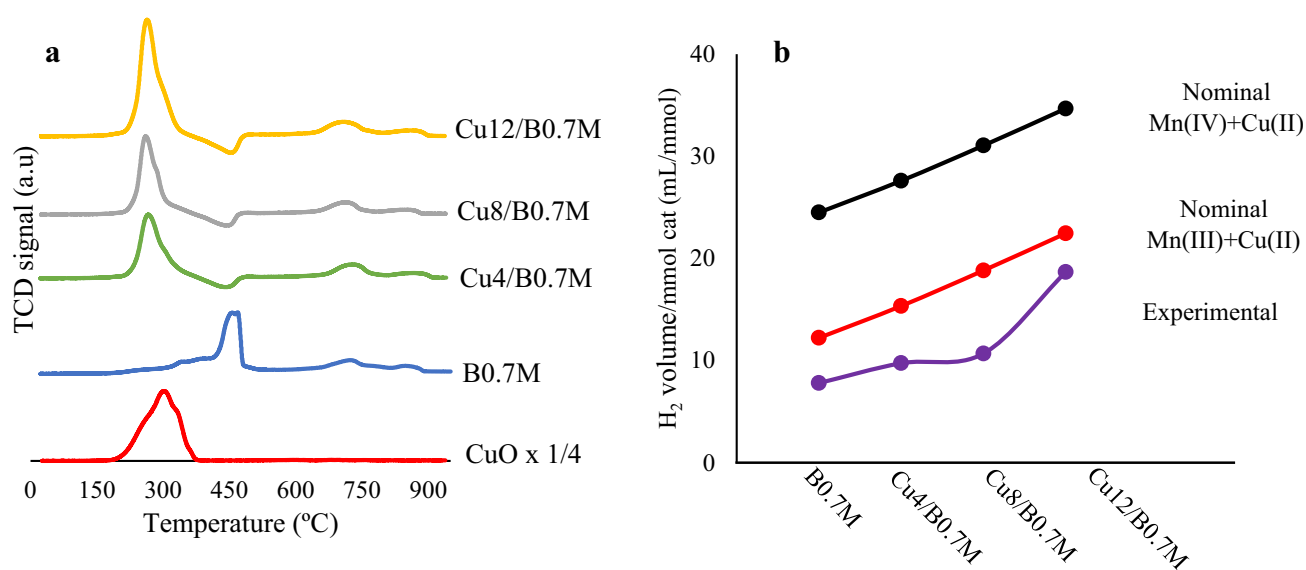
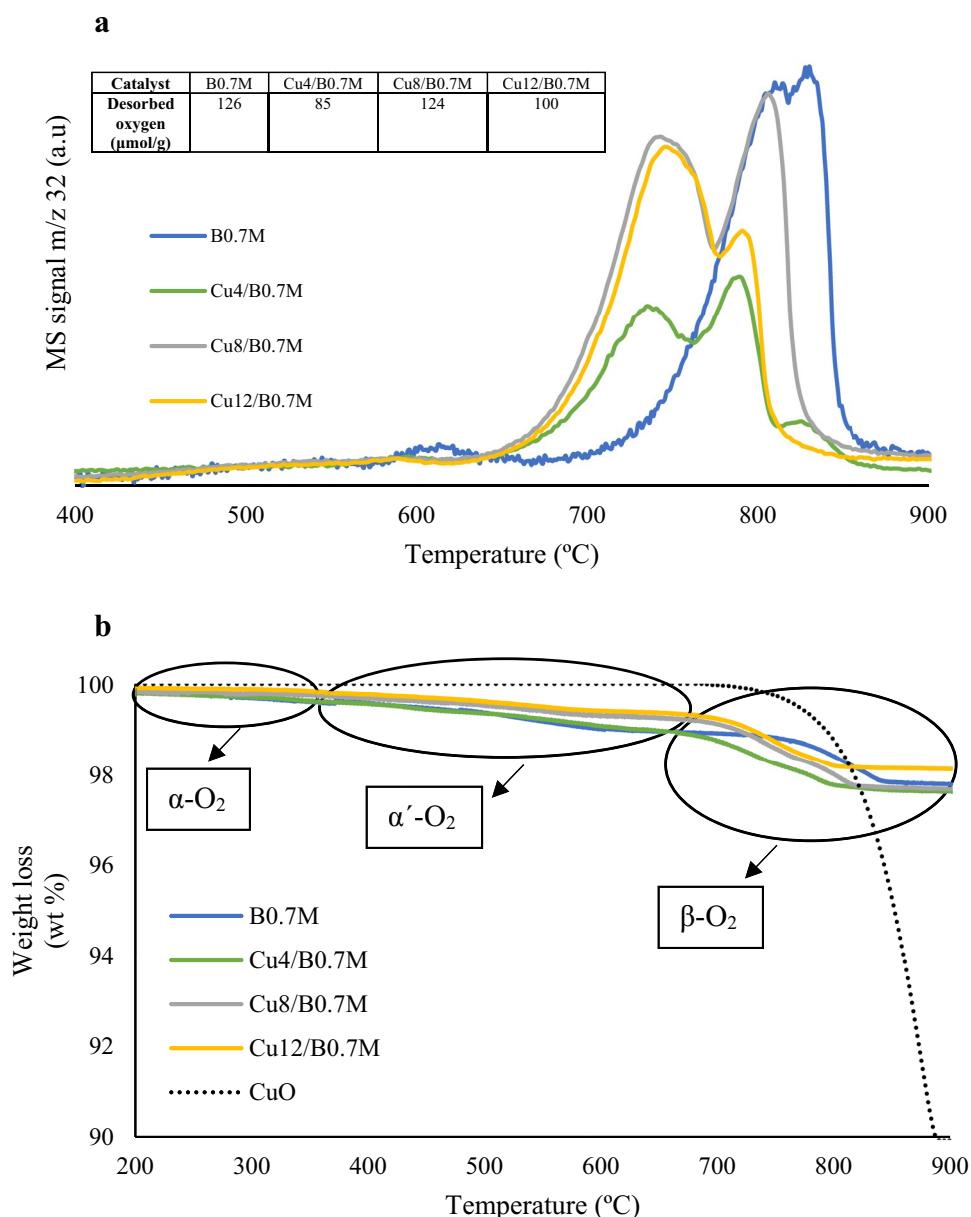


Fig. 5 H_2 -TPR consumption profiles for the catalysts and the CuO reference sample (a) and H_2 consumption (mL/mmol of catalyst) (b)

Fig. 6 **a** O₂-TPD profiles and **b** weight loss profiles of the B0.7M and CuX/B0.7M catalysts



ratios shown in Table 2], so it should contain CuO particles with the largest average size and, consequently, will evolve a lower amount of β -O₂. In conclusion, the presence of copper decreases the total amount of oxygen evolved (except for Cu8/B0.7M) but allows the evolution of β -O₂ at lower temperatures than the perovskite support due to the presence of CuO phase, thus, increasing the oxygen mobility.

The weight loss profiles during the O₂-TPD experiment for B0.7M and CuX/B0.7M catalysts are presented in Fig. 6b, including the corresponding to a CuO sample used as reference. The loss of weight registered for all samples is mainly due to the release of the different oxygen species present in perovskite samples. Note that the most significant weight loss takes place over 700 °C, so, it is associated to the

evolution of lattice oxygen (β -O₂). Additionally, the other very small weight loss observed in Fig. 6b correspond to: (i) chemisorbed water release at low temperatures, (ii) thermal decomposition of BaCO₃ (to BaO and CO₂) at approximately 815 °C [34] and (c) the reduction of CuO to Cu₂O (which takes place over 700 °C in inert atmosphere [35]) observed for the CuX/B0.7M catalysts.

3.5 Catalytic Activity

Figure 7a and b shows the CO conversion profiles obtained for the catalysts in the two reaction mixtures tested (see Experimental section for details) and Table 4 features the temperature required to reach 50% of CO conversion ($T_{50\%}$).

Figure 7 reveals that all catalysts are active for CO oxidation in the two conditions used, as CO is not converted to CO₂ in the absence of catalysts (denoted as blank in the figure). However, at low CO content mixture (0.1% CO, 1% O₂), the copper-supported catalysts show a lower activity than the perovskite support (Fig. 7a). The opposite is observed in Fig. 7b for stoichiometric mixture (1% CO, 1% O₂), as CuX/B0.7M catalysts are more active than the B0.7M support, even though, the CO conversion does not linearly increase with copper content and Cu8/B0.7M presents the lowest activity. The low activity of Cu8/B0.7M could be related with the lower reducibility observed during H₂-TPR (Fig. 5), as consequence of the lower amount of surface copper species with a strong interaction with perovskite support

Fig. 7 CO-TPR conversion profiles for B0.7M and CuX/B0.7M catalysts in: **a** 0.1% CO, 1% O₂ in He; **b** 1% CO, 1% O₂ in He

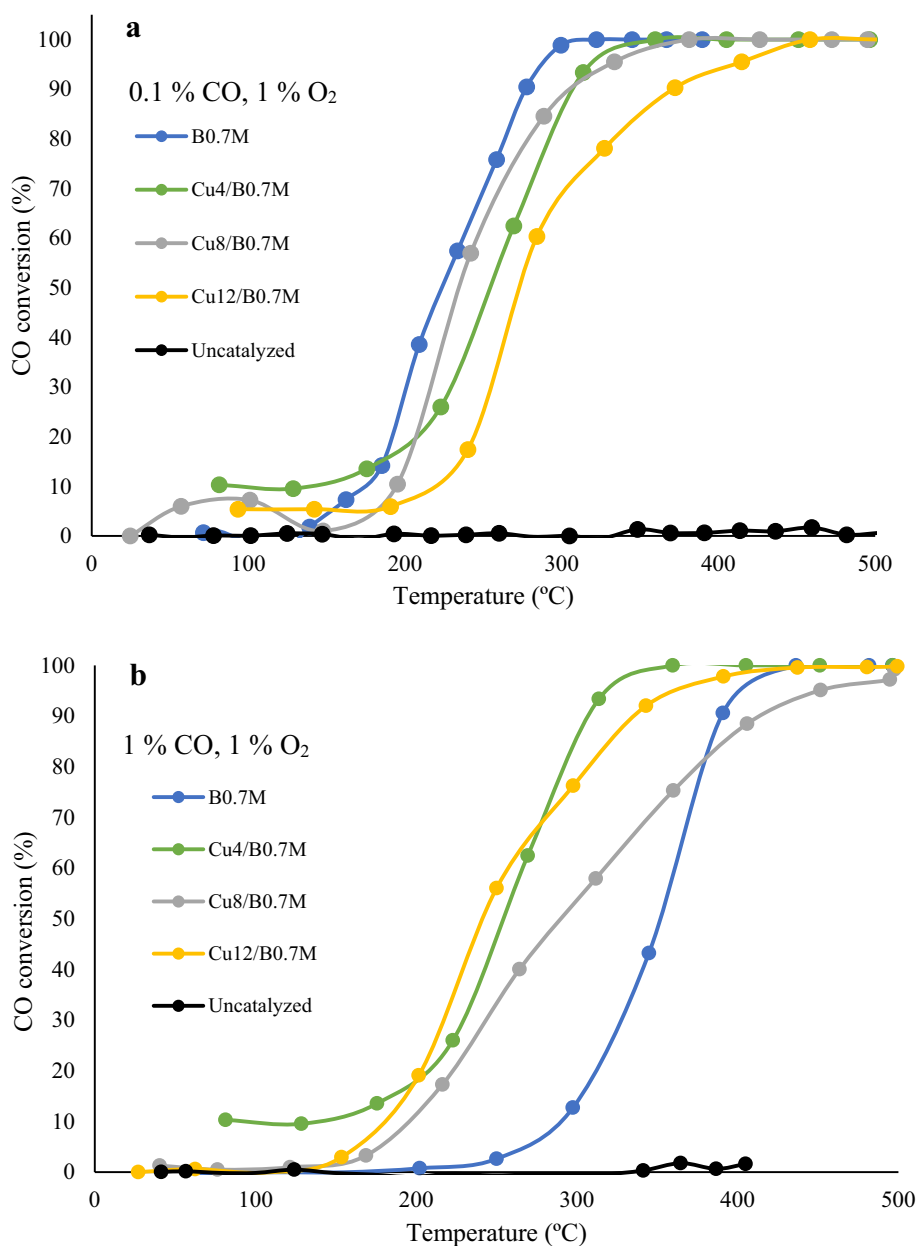
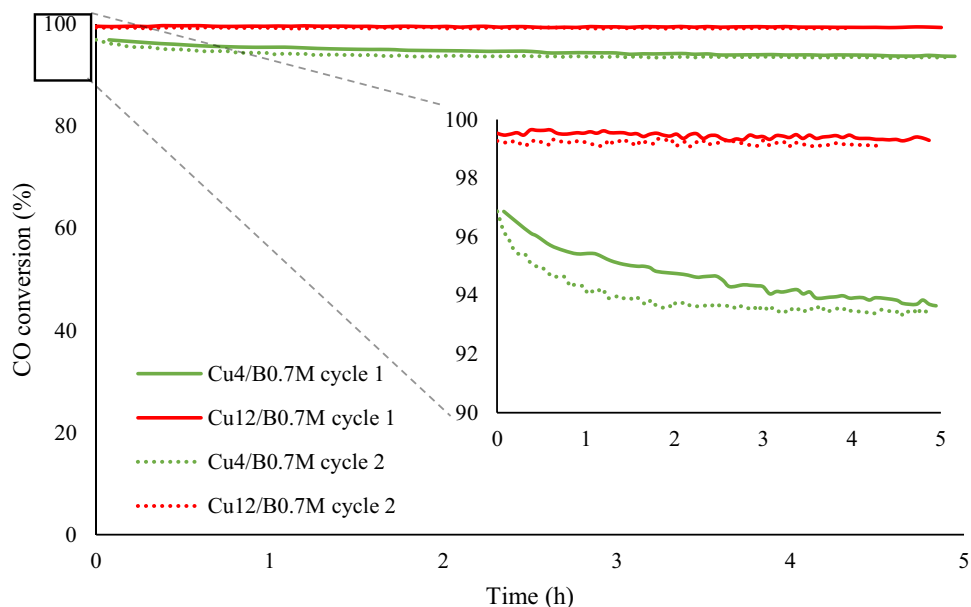


Table 4 T_{50%} values for B0.7M and CuX/B0.7M catalysts

| Catalyst | T _{50%} (0.1% CO, 1% O ₂) (°C) | T _{50%} (1% CO, 1% O ₂) (°C) |
|------------|---|---|
| B0.7M | 224 | 351 |
| Cu4/B0.7M | 253 | 253 |
| Cu8/B0.7M | 234 | 291 |
| Cu12/B0.7M | 274 | 242 |

respect to the other two catalysts (see XPS data in Table 2). On the other hand, comparing T_{50%} values for the two reactant mixtures tested, it is observed that: (i) T_{50%} increases for CO rich mixture for B0.7M and for Cu8/B0.7M, being

Fig. 8 CO conversion profiles at 300°C for Cu4/B0.7M and Cu12/B0.7M catalysts



the increase higher for the perovskite support than for the copper catalyst and (ii) it is not modified for Cu4/B0.7M and for Cu12/B0.7M catalysts, being even lower in the rich CO mixture. Considering the data for surface composition obtained by XPS (Table 2), it seems that the CuX/B0.7M catalysts with a high proportion of surface copper with a strong interaction with perovskite, as Cu4/B0.7M and Cu12/B0.7M, would be more stable against the fluctuations in the composition of the exhaust mixture evolved by GDI engines.

For the two catalysts revealing as the most active in the near stoichiometric conditions (1% CO, 1% O₂), that is, Cu4/B0.7M and Cu12/B0.7M, two cycles of CO oxidation at 300 °C were performed, being the profiles shown in Fig. 8. The CO conversion percentages for these two catalysts, that are similar to the observed in the Temperature-Programmed Reaction conditions (CO-TPR in Fig. 7), remain almost constant during reaction time at 300 °C and for the two cycles carried out, so, the two catalysts present and high stability and recyclability.

Nevertheless, it is observed that Cu4/B0.7M shows a slight deactivation during the reaction time. According to literature [43, 44], the deactivation could be related with the carbonate formation on the perovskite surface which modifies the interaction of reactants with the active sites. In order to obtain information about the potential modification of the surface during reaction, the two used catalysts were analyzed by XPS after first reaction cycle at 300 °C, being the most relevant results shown in Tables 5 and 6. The amount of barium carbonate (calculated based on the deconvolution of Ba 3d^{5/2} XPS band corresponding to this species) is not significantly modified after reaction, so, the formation of barium carbonate seems not to be causing the slight deactivation. For both catalysts, the

Table 5 Ba and Mn XPS characterization data of the Cu4/B0.7M and Cu12/B0.7M used catalysts (data for fresh catalysts in brackets)

| Catalyst | BaCO ₃ (% wt) | Mn(IV)/Mn(III) | Mn(III) _i /Mn(III) _f |
|------------|--------------------------|----------------|--|
| Cu4/B0.7M | 11 (14) | 1.1 (1.3) | 0.3 (0.2) |
| Cu12/B0.7M | 10 (9) | 1.3 (1.4) | 0.9 (0.2) |

Table 6 Cu and O XPS characterization data of the Cu4/B0.7M and Cu12/B0.7M used catalysts (data for fresh catalysts in brackets)

| Catalyst | Experimental Cu/(Ba + Mn + Cu) | Cu _{si} /Cu _{wi} | O _L /(Ba + Mn) |
|------------|--------------------------------|------------------------------------|---------------------------|
| Cu4/B0.7M | 0.14 (0.10) | 0.5 (1.6) | 1.3 (1.4) |
| Cu12/B0.7M | 0.21 (0.18) | 1.0 (1.3) | 1.4 (1.3) |

Cu/(Ba + Mn + Cu) XPS ratio increases during reaction (suggesting that the decrease in CO conversion could be related with a lower amount of CuO active sites due to particles sintering) and the Mn(IV)/Mn(III) ratio decreases. Note that the sintering process seems to decrease the Cu_{si}/Cu_{wi} ratio more significantly for Cu4/B0.7M catalyst. So, it seems that the surface copper species with a strong interaction with the support promote a higher catalytic activity and stability than those with a weak interaction with the perovskite. Thus, as the two modifications observed are more significant for Cu4/B0.7M than for Cu12/B0.7M, so Cu4/B0.7M catalyst experiments more relevant changes during the reaction than Cu12/B0.7M catalyst, and this fact could justify its slightly lower stability during reaction time. However, these modifications do not affect the

recyclability as the two catalysts show almost the same performance during the second reaction cycle.

According to literature, two mechanisms for catalyzed CO oxidation reaction are accepted [41]: (i) the Langmuir–Hinshelwood mechanism which implies a reaction between the two adsorbed reactants, and (ii) the Eley–Rideal mechanism which proposes that reaction takes place with only one of the reactant adsorbed on the catalyst surface. In previous studies [27], it has been concluded that the Langmuir–Hinshelwood mechanism works for catalyzed CO oxidation in the presence of oxygen vacancies, in which the preferential adsorption of O₂ on oxygen vacancies takes place to form highly active O⁻¹ species [27, 42]. Accepting this mechanism is working, the following discussion of the results for both reactant mixtures could be offered:

- (i) In the low CO mixture (0.1% CO, 1% O₂), oxygen is preferably chemisorbed on the surface oxygen vacancies/defects (forming active O⁻¹) as it is in excess and, after, the CO molecules are also adsorbed on the free oxygen defects (not occupied active sites). So, oxygen defects seem being the active sites and, consequently, CO conversion decreases for copper-containing catalysts, due to their lower amount of oxygen defects on surface (Table 3).
- (ii) In near stoichiometric conditions (1% CO, 1% O₂), as the CO concentration is higher (1% versus 0.1%), the surface CuO species seem working also as active sites and, consequently, the CO conversion increases in the presence of copper.

Finally, the catalytic performance of CuX/B0.7M catalysts series has been compared with the corresponding to two previously studied catalysts series with stoichiometric composition, i.e., BaMn_{1-x}Cu_xO₃ and CuX/BaMnO₃ [40]:

- B0.7M catalyst shows a higher catalytic activity (T_{50%} = 224 °C) than stoichiometric BaMnO₃ perovskite (T_{50%} = 280 °C) synthesized by using the sol–gel method (named BM) for low CO gas mixture (0.1% CO, 1% O₂), because the amount of surface oxygen vacancies is higher in B0.7M than in BM. However, in 1% CO, the catalytic activity of B0.7M perovskite (T_{50%} = 351 °C) is lower than for BM catalyst (T_{50%} = 320 °C), revealing that the barium-deficient perovskite is more affected than the stoichiometric perovskite (BM) by the increase in the CO concentration. Thus, as it has been discussed above, the addition of copper to B0.7M seems to solve this drawback because it increases the activity of CuX/B0.7M catalysts in 1% CO/ 1% O₂ atmosphere, as surface CuO species seems to act also as active sites.
- All the CuX/B0.7M catalysts (Table 4) show a better catalytic performance in the two reactant mixtures than the

stoichiometric BaMn_{0.7}Cu_{0.3}O₃ perovskite obtained by the sol–gel method (named BMC3), with T_{50%} of 280 °C and 295 °C for 0.1% CO and 1% CO, respectively. This is because a lower amount of CuO active sites exists on the surface of BaMn_{0.7}Cu_{0.3}O₃ perovskite than on the surface of CuX/B0.7M catalysts.

- Finally, the catalytic activity of 7.8-Cu/BM (obtained by impregnation of the stoichiometric perovskite BM) is higher (T_{50%} of 210 °C and 205 °C for 0.1% CO and 1% CO, respectively) than the found for any of the CuX/B0.7M catalysts series (see Table 4), as the amount of oxygen defects (acting as active sites) is higher for 7.8-Cu/BM than for CuX/B0.7M.

Torregrosa et al. [40] probed that by using hydrothermal method for the synthesis of BM and BMC3 (denoted as BM-H and BMC3-H), the catalytic performance is improved respect to the BM and BMC3 catalysts, as this synthesis procedure allows a barium deficiency for BaMnO₃ perovskites. Thus, the next step for optimizing the catalytic activity of B0.7M perovskite for CO oxidation in near stoichiometric conditions will be the synthesis of this formulation by hydrothermal method. After the optimization, the catalytic performance of this perovskite formulation for CO oxidation under more realistic conditions, as well as for other applications (i.e. CO preferential oxidation reaction, CO-PROX, commonly employed as an effective procedure for removing CO in H₂-rich gas mixtures generated by reforming processes, to be used in fuel cells [43, 45–48]) should be explored.

4 Conclusions

The Ba_{0.7}MnO₃ perovskite synthesized using the sol–gel method has been used as support to prepare a series of Cu impregnated catalysts (4, 8 and 12 wt%).

The characterization results reveal that Cu is located on the perovskite surface as CuO, which partially covers the oxygen defects of the perovskite and promotes the Mn(III) oxidation to Mn(IV) on the surface.

CuO improves the reducibility of the perovskite through a Mn–Cu synergic effect, and the release of β-O₂ (oxygen from the lattice of perovskite) which enhances oxygen mobility through perovskite.

The presence of CuO allows increasing the catalytic activity for the CO oxidation in ideal near stoichiometric conditions (1% CO, 1% O₂ in He), as the CuO participates in the activation of CO and O₂ as active site. Consequently, the presence of CuO increases the stability of the catalysts against the reactant concentration fluctuations, and it induces a higher stability and recyclability in isothermal conditions, being the most active catalysts those presenting a high

proportion of copper with a strong interaction with the perovskite support.

Funding Open Access funding provided thanks to the CRUE-CSIC agreement with Springer Nature. This work was supported by Ministerio de Ciencia, Innovación y Universidades, (Grant No. PID2019-105542RB-I00), María José Illán Gómez, European Regional Development Fund, Generalitat Valenciana, (Grant No. CIPROM/2021-070 project), María José Illán Gómez, Universidad de Alicante

Declarations

Conflict of interest This study was funded by the Spanish Government (MINCINN: PID2019-105542RB-I00 Project), the European Union (FEDER Funds,) the Regional Government (Generalitat Valenciana CIPROM/2021-070 project) and the University of Alicante (Final Master's Project grant of A. Díaz-Verde).

Open Access This article is licensed under a Creative Commons Attribution 4.0 International License, which permits use, sharing, adaptation, distribution and reproduction in any medium or format, as long as you give appropriate credit to the original author(s) and the source, provide a link to the Creative Commons licence, and indicate if changes were made. The images or other third party material in this article are included in the article's Creative Commons licence, unless indicated otherwise in a credit line to the material. If material is not included in the article's Creative Commons licence and your intended use is not permitted by statutory regulation or exceeds the permitted use, you will need to obtain permission directly from the copyright holder. To view a copy of this licence, visit <http://creativecommons.org/licenses/by/4.0/>.

References

- Climate Change. Climate Action. <https://www.un.org/en/climatechange/what-is-climate-change>. Accessed 10 Jan 2022.
- Paris Agreement. https://ec.europa.eu/clima/policies/international/negotiations/paris_es. Accessed 10 Jan 2022.
- Bloomberg New Energy Finance, "New Energy Outlook 2021" report. <https://about.bnef.com/new-energy-outlook/>. Accessed 2 Jul 2022.
- Hanaki Y, Fujimoto M, Ito J (2016) Alternative technology for platinum group metals in automobile exhaust gas catalysts. SAE Technical Paper. <https://doi.org/10.4271/2016-01-0930>
- Theis JR, Getsoian A, Lambert C (2017) The developments of low temperature three-way catalysts for high efficiency gasoline engines of the future. SAE Int J Fuels Lubr 10:583–592. <https://doi.org/10.4271/2017-01-0918>
- Peña MA, Fierro JLG (2001) Chemical structures and performance of perovskite oxides. Chem Rev 101:1981–2018. <https://doi.org/10.1021/cr980129f>
- Yadav P, Yadav S, Atri S, Tomar R (2021) A brief review of key role of perovskite oxides as catalyst. ChemistrySelect 6:12947–12959. <https://doi.org/10.1002/slct.202102292>
- Wang K, Han C, Shao Z, Qiu J, Wang S, Liu S (2021) Perovskite oxide catalysts for advanced oxidation reactions. Adv Funct Mater 31:2102089. <https://doi.org/10.1002/adfm.202102089>
- Peron G, Glisenti A (2018) Perovskites as alternatives to noble metals in automotive exhaust abatement: activation of oxygen on LaCrO₃ and LaMnO₃. Top Catal 62:244–251. <https://doi.org/10.1007/s11244-018-1120-1>
- Díaz-Verde A, Torregrosa-Rivero V, Sánchez-Adsuar MS, Illán-Gómez MJ. In *Catalizadores basados en Ba_xMnO₃ para la oxidación de CO*, Proceedings of the IV Encuentro de Jóvenes Investigadores de la SECAT, Bilbao, Spain, Sep 21–23, 2020.
- Torregrosa-Rivero V, Albadejo-Fuentes V, Sánchez-Adsuar MS, Illán-Gómez MJ (2017) Copper doped BaMnO₃ perovskite catalysts for NO oxidation and NO₂-assisted diesel soot removal. RSC Adv 7:35228–35238. <https://doi.org/10.1039/C7RA04980C>
- Flores-Lasluisa JX, Huerta F, Cazorla-Amorós D, Morallón E (2019) Structural and morphological alterations induced by cobalt substitution in LaMnO₃ perovskites. J Colloid Interface Sci 556:658–666. <https://doi.org/10.1016/j.jcis.2019.08.112>
- Campagnoli E, Tavares A, Fabbrini L, Rossetti I, Dubitsky YA, Zaopo A, Forni L (2005) Effect of preparation method on activity and stability of LaMnO₃ and LaCoO₃ catalysts for the flameless combustion of methane. Appl Catal B 55:133–139. <https://doi.org/10.1016/j.apcatb.2004.07.010>
- Torregrosa-Rivero V, Moreno-Marcos C, Albaladejo-Fuentes V, Sánchez-Adsuar MS, Illán-Gómez MJ (2019) BaFe_{1-x}Cu_xO₃ perovskites as active phase for diesel (DPF) and gasoline particle filters (GPF). Nanomaterials 9:1551. <https://doi.org/10.3390/nano9111551>
- Hu Y, Han X, Zhao Q, Du J, Cheng F, Chen J (2015) Porous perovskite calcium-manganese oxide microspheres as an efficient catalyst for rechargeable sodium-oxygen batteries. J Mater Chem A 3:3320–3324. <https://doi.org/10.1039/C4TA06287F>
- Ulyanov AN, Yu SC, Yang DSJ (2004) Mn-site-substituted lanthanum manganites: destruction of electron pathway and local structure effects on curie temperature. J Magn Magn Mater 282:303–306. <https://doi.org/10.1016/j.jmmm.2004.04.071>
- Islam SAU, Ikram M (2019) Structural stability improvement, Williamson Hall analysis and band-gap tailoring through A-site Sr doping in rare earth based double perovskite La₂NiMnO₆. Rare Met 38:805–813. <https://doi.org/10.1007/s12598-019-01207-4>
- Sahoo B, Joseph J, Sharma A, Paul J (2017) Surface modification of aluminium by graphene impregnation. Mater Des 116:51–64. <https://doi.org/10.1016/j.matdes.2016.11.075>
- XPS Simplified. <https://xpsimplified.com>. Accessed 21 Jan 2021.
- Luo L, Huang H, Yang Y, Gong S, Li Y, Wang Y, Luo W, Li Z (2022) Nickel and manganese oxide heterostructure nanoparticles supported by carbon nanotube for highly efficient oxygen evolution reaction catalysis. Appl Surf Sci 575:151699. <https://doi.org/10.1016/j.apsusc.2021.151699>
- Shen Q, Zhou J, Ma C, Yang J, Cao L, Yang J (2022) Development of LnMnO_{3+δ} perovskite on low temperature H₂O removal. J Environ Sci 113:141–151. <https://doi.org/10.1016/j.jes.2021.04.007>
- Chen J, Shen M, Wang X, Qi G, Wang J, Li W (2013) The influence of nonstoichiometry on LaMnO₃ perovskite for catalytic NO oxidation. Appl Catal B 134–135:251–257. <https://doi.org/10.1016/j.apcatb.2013.01.027>
- López-Suárez FE, Bueno-López A, Illán-Gómez MJ, Trawczynski J (2014) Potassium-copper perovskite catalysts for mild temperature diesel soot combustion. Appl Catal A 485:214–221. <https://doi.org/10.1016/j.apcata.2014.07.037>
- LaSurface Database. <https://lasurface.com>. Accessed 22 Mar 2021.
- Tabata K, Hirano Y, Suzuki E (1998) XPS studies on the oxygen species of LaMn_{1-x}Cu_xO_{3+λ}. Appl Catal A 170:245–254. [https://doi.org/10.1016/S0926-860X\(98\)00062-3](https://doi.org/10.1016/S0926-860X(98)00062-3)
- Albaladejo-Fuentes V, López-Suárez FE, Sánchez-Adsuar MS, Illán-Gómez MJ (2016) Tailoring the properties of BaTi_{0.8}Cu_{0.2}O₃ catalyst selecting the synthesis method. Appl Catal A 519:7–15. <https://doi.org/10.1016/j.apcata.2016.03.022>
- Yang J, Hu S, Fang Y, Hoang S, Li L, Yang W, Liang Z, Wu J, Hu J, Xiao W, Pan C, Luo Z, Ding J, Zhang L, Guo Y (2019) Oxygen vacancy promoted O₂ activation over perovskite oxide for

- low-temperature CO oxidation. *ACS Catal* 9:9751–9763. <https://doi.org/10.1021/acscatal.9b02408>
28. López-Suárez FE, Parres-Esclapez S, Bueno-López A, Illán-Gómez MJ, Trawczynski J (2009) Role of surface and lattice copper species in copper-containing (Mg/Sr)TiO₃ perovskite catalysts for soot combustion. *Appl Catal B* 93:82–89. <https://doi.org/10.1016/j.apcatb.2009.09.015>
 29. Albaladejo-Fuentes V, López-Suárez F, Sánchez-Adsuar MS, Illán-Gómez MJ (2017) BaTi_{0.8}Cu_{0.2}O₃ catalysts for NO oxidation and NO_x storage: effect of synthesis method. *Top Catal* 60:220–224. <https://doi.org/10.1007/s11244-016-0601-3>
 30. Wang W, Yuan F, Niu X, Zhu Y (2016) Preparation of Pd supported on La(Sr)-Mn-O perovskite by microwave irradiation method and its catalytic performances for the methane combustion. *Sci Rep* 6:19511. <https://doi.org/10.1038/srep19511>
 31. Zhang R, Alamdari H, Kaliaguine S (2006) Fe-based perovskites substituted by copper and palladium for NO + CO reaction. *J Catal* 242:241–253. <https://doi.org/10.1016/j.jcat.2006.05.033>
 32. Huang C, Zhu Y, Wang X, Liu X (2017) Sn promoted BaFeO_{3-δ} catalysts for N₂O decomposition: optimization of Fe active centers. *J Catal* 347:9–20. <https://doi.org/10.1016/j.jcat.2016.12.020>
 33. Gan R, Nishida Y, Haneda M (2022) Effect of B-site substitution on the catalytic activity of La-based perovskite for oxidative coupling of methane. *Phys Status Solidi B*. <https://doi.org/10.1002/pssb.202100544>
 34. Albaladejo-Fuentes V, Sánchez-Adsuar MS, Anderson JA, Illán-Gómez MJ (2021) NO_x storage on BaTi_{0.8}Cu_{0.2}O₃ perovskite catalysts: addressing a feasible mechanism. *Nanomaterials* 11:2133. <https://doi.org/10.3390/nano11082133>
 35. Giménez-Mañogil J, García-García A (2017) Identifying the nature of the copper entities over ceria-based supports to promote diesel soot combustion: synergistic effects. *Appl Catal A* 542:226–239. <https://doi.org/10.1016/j.apcata.2017.05.031>
 36. Balamurugan S, Mini KSA, Raja TSG, Parthiban P (2015) Mechano-thermal synthesis and characterization of BaMnO₃ nanoneedles. *J Nanosci Nanotechnol* 15:5978–5986. <https://doi.org/10.1166/jnn.2015.10196>
 37. Gao F, Lewis RA, Wang XL, Dou SX (2002) Far-infrared reflection and transmission of La_{1-x}Ca_xMnO₃. *J Alloys Compd* 347:314–318. [https://doi.org/10.1016/S0925-8388\(02\)00789-2](https://doi.org/10.1016/S0925-8388(02)00789-2)
 38. Roy C, Budhani RC (1998) Raman- and infrared-active phonons in hexagonal BaMnO₃. *Phys Rev B* 58:8174–8177. <https://doi.org/10.1103/PhysRevB.58.8174>
 39. Chen L, Li L, Li G (2008) Synthesis of CuO nanorods and their catalytic activity in the thermal decomposition of ammonium perchlorate. *J Alloys Compd* 464:532–536. <https://doi.org/10.1016/j.jallcom.2007.10.058>
 40. Torregrosa-Rivero V. BaMnO₃ perovskite-based catalysts for pollution control generated by highly efficient automotive engines. PhD tesis, University of Alicante, Sep 2021, pp 283, 327. <http://hdl.handle.net/10045/120794>
 41. Zhang-Steenwinkel Y, van der Zande LM, Castricum HL, Blik A (2004) Step response and transient isotopic labelling studies into the mechanism of CO oxidation over La_{0.8}Ce_{0.2}MnO₃ perovskite. *Appl Catal B* 54:93–103. <https://doi.org/10.1016/j.apcatb.2004.02.008>
 42. Loc LC, Tri N, Cuong HT, Gaidai NA, Agafonov YA, Nekrasov NV, Anh HC, Thoang HS, Lapidus AL (2014). In *Mechanism of carbon monoxide oxidation over supported CuO catalysts modified by Ce and Pt*. DGMK Tagungsbericht 3:167–173. https://www.researchgate.net/publication/287267863_Mechanism_of_carbon_monoxide_oxidation_over_supported_CuO_catalysts_modified_by_Ce_and_Pt
 43. Schmal M, Perez CAC, Magalhães RNSH (2014) Synthesis and characterization of perovskite-type oxides La_{1-x}M_xCoO₃ (M = Ce, Sr) for the selective CO oxidation (SELOX). *Top Catal* 57:1103–1111. <https://doi.org/10.1007/s11244-014-0275-7>
 44. Mokoena L, Pattrick G, Scurrill MS (2016) Catalytic activity of gold-perovskite catalysts in the oxidation of carbon monoxide. *Gold Bull* 49:35–44. <https://doi.org/10.1007/s13404-016-0180-x>
 45. Martínez-Munuera JC, Giménez-Mañogil J, Yeste MP, Hungría AB, Cauqui MA, García-García A, Calvino JJ (2022) New findings regarding the role of copper entity particle size on the performance of Cu/ceria-based catalysts in the CO-PROX reaction. *Appl Surf Sci* 575:151717. <https://doi.org/10.1016/j.apsusc.2021.151717>
 46. Beckers J, Rothenberg G (2010) Sustainable selective oxidations using ceria-based materials. *Green Chem* 12:939–948. <https://doi.org/10.1039/C000191K>
 47. Tapia-P J, Gallego J, Espinal JF (2021) Calcination temperature effect in catalyst reactivity for the CO SELOX reaction using perovskite-like LaBO₃ (B: Mn, Fe Co, Ni) oxides. *Catal Lett* 151:3690–3703. <https://doi.org/10.1007/s10562-021-03601-z>
 48. Chagas CA, Magalhães RNSH, Schmal M (2021) The LaCo_{1-x}V_xO₃ catalyst for CO oxidation in rich H₂ stream. *Catal Lett* 151:409–421

Publisher's Note Springer Nature remains neutral with regard to jurisdictional claims in published maps and institutional affiliations.